Inviscid coupling between point symmetric bodies and singular distributions of vorticity

I. EAMES, M. LANDERYOU and J. B. FLÓR

Journal of Fluid Mechanics / Volume 589 / October 2007, pp 33 - 56
DOI: 10.1017/S0022112007007161, Published online: 08 October 2007

J. Fluid Mech. (2007), *vol.* 589, *pp.* 33–56.
doi:10.1017/S0022112007007161 Printed in the United Kingdom

Inviscid coupling between point symmetric bodies and singular distributions of vorticity

I. EAMES[1], M. LANDERYOU[1] AND J. B. FLÓR[2]

[1]Departments of Mechanical Engineering and Mathematics, University College London, Torrington Place, London, WC1E 7JE, UK

[2]Laboratoires des Ecoulement Geophysiques et Industriels, BP 53, 38041, Grenoble Cedex 09, France

(Received 17 May 2004 and in revised form 16 May 2007)

We study the inviscid coupled motion of a rigid body (of density ρ_b, in a fluid of density ρ) and singular distributions of vorticity in the absence of gravity, using for illustration a cylinder moving near a point vortex or dipolar vortex, and the axisymmetric interaction between a vortex ring and sphere.

The coupled motion of a cylinder (radius a) and a point vortex, initially separated by a distance R and with zero total momentum, is governed by the parameter $R^4/(\rho_b/\rho + 1)a^4$. When $R^4/(\rho_b/\rho+1)a^4 \ll 1$, a (positive) point vortex moves anticlockwise around the cylinder which executes an oscillatory clockwise motion, with a mixture of two frequencies, centred around its initial position. When $R^4/(\rho_b/\rho + 1)a^4 \gg 1$, the initial velocity of the cylinder is sufficiently large that the dynamics become uncoupled, with the cylinder moving off to infinity. The final velocity of the cylinder is related to the permanent displacement of the point vortex.

The interaction between a cylinder (initially at rest) and a dipolar vortex starting at infinity depends on the distance of the vortex from the centreline (h), the initial separation of the vortical elements ($2d$), and ρ_b/ρ. For a symmetric encounter ($h = 0$) with a dense cylinder, the vortical elements pass around the cylinder and move off to infinity, with the cylinder being displaced a finite distance forward. However, when $\rho_b/\rho < 1$, the cylinder is accelerated forward to such an extent that the vortex cannot overtake. Instead, the cylinder 'extracts' a proportion of the impulse from the dipolar vortex. An asymmetric interaction ($h > 0$) leads to the cylinder moving off in the opposite direction to the dipolar vortex.

To illustrate the difference between two- and three-dimensional flows, we consider the axisymmetric interaction between a vortex ring and a rigid sphere. The velocity perturbation decays so rapidly with distance that the interaction between the sphere and vortex ring is localized, but the underlying processes are similar to two-dimensional flows.

We briefly discuss the general implications of these results for turbulent multiphase flows.

1. Introduction

A Lagrangian formulation of fluid mechanics is based on following 'identifiable pieces of matter' (Batchelor 1967, p. 71). While much simpler than an Eulerian formulation to pose, it tends to be difficult to apply because of the large number of pieces of 'matter' to be followed. (These two formulations were conveniently

designated by German mathematicians as the 'Eulerian' and the 'Lagrangian' forms, although in reality, both are due to Euler (Lamb 1932).) In a Lagrangian formulation of a dispersed multiphase flow, the 'pieces of matter' (bubbles, droplets or particles) are followed by integrating with time the force and torque acting on them; the force and torque are estimated from the local values of the flow and the velocity gradient tensor to give the instantaneous velocity and acceleration of the particles (see Magnaudet & Eames 2000, for a review of some of these forces). Most semi-empirical expressions for force and torque used are based on the requirement that the pieces of 'matter' are much smaller than the characteristic length scale of the local flow into which they move. For turbulent flows, this requires particles to be smaller than the Kolmogorov length scale characterizing the smallest eddies through which the particles move. Extensive progress has been made when this criterion is strictly valid (see the review by Squires & Simonin 2002).

A turbulent or unsteady flow generated by discrete elements or particles can create flow features on a scale comparable to, or even smaller than the elements themselves owing to vortex shedding and wake instabilities (e.g. Hill, Koch & Ladd 2001; Mougin & Magnaudet 2002). These particles will experience unsteady lift and drag forces by shedding vorticity (Sarpkaya 1963, 1968), as well as from their interaction with vortices shed from particles upstream. These forces are significant for particles whose density is comparable to, or less than, the ambient fluid. Under these circumstances, the particles are not much smaller than the local length scale associated with the upstream flow, and the estimates of the force and torque, generally used in Lagrangian formulations of multiphase flows (see Magnaudet & Eames 2000), may no longer be suitable. The first major question is what is the force on particles moving in the vicinity of flow structures, such as vortices, which are of comparable size or smaller than the particles. The second question is how do the particles themselves permanently affect the flow.

The interaction between rigid bodies and vortices has been studied extensively for inviscid fluids. Solutions describing point and dipolar vortices interacting with fixed planar bodies (or bodies of infinite density) are described by Milne-Thompson (1968). To quantify the unsteady force on riser pipes, Sarpkaya (1963, 1968) studied the interaction between a cylinder and point vortices representing previously shed vorticity which interacts with the cylinder. Dhanak (1981) and Pedrizzetti (1992) examined the unsteady interaction between a sphere and vortex filament. Howe, Lauchle & Wang (2001) analysed the frequency spectra of the force generated by vortex shedding from a sphere, and their comparison with experimental results was good. These studies have been extended using direct numerical simulation (DNS) to examine how pairs of line vortices interact with a sphere (Kim, Elghobashi & Sirignano 1997) or the influence of a line vortex on the heat and mass transfer rates from spherical droplets (Masoudi & Sirignano 2000). The force on the rigid body in the presence of vortices can be estimated from these studies, but the dynamic coupling and the communication of momentum/impulse between the body and vortices is not understood. This forms an essential element of this paper.

Some nonlinear aspects of turbulence can be understood from the dynamics of rigid particles in inhomogeneous flows. A mechanistic approach was first applied by Rossby (1948), and later by Flór & Eames (2002), to explain the influence of gradients in the Coriolis force on the trajectory of monopolar vortices. Hunt (1987) considered the dynamics of rigid bodies in sheared flows, and furthered Prandtl's 'fluid-lump' approach to interpret Reynolds stress. Examples of vortices interacting with small-scale structures are large eddies interacting with thin boundary layers (Smedman, Hogstrom & Hunt 2003), turbulence interacting with sharp shear layers, and vortices

impinging on density interfaces (Linden 1973). Shear layers tend to inhibit cross-zonal transport and act as barriers to transport (see Juckes & McIntyre 1987), as observed at the edge of the polar vortex. Hunt & Durbin (1999) studied the motion of a vortex (or 'fluid-lump') near a shear layer and suggested that shear layers shelter one region from another and inhibit the movement of vortices across the layer. Although we focus on the coupled motion of rigid bodies and vortices, the general processes described are also relevant to understanding the 'shear sheltering' mechanism.

To understand the coupled motion between rigid bodies and a rotational flow, we focus on singular distributions of vorticity in an inviscid flow in the absence of buoyancy forces. The force on a cylinder moving near a collection of point vortices was calculated by Sarpkaya & Garrison (1963), Shashikanth *et al.* (2002), Borisov & Mamaev (2003), and Ramodanov (2002), while the coupled dynamics of a single-point vortex and a cylinder were reported by Ramodanov (2001). The analysis of Shashikanth *et al.* (2002) is noteworthy because they developed a Hamiltonian formulation for circular cylinders interacting with point vortices, which they applied to comment on the stability of Föppl's wake vortices. Shashikanth (2006) examined the dynamics of a cylinder of the same density as the ambient fluid, interacting with point vortices and studied the vortex trajectories and stability of the coupled motion, using a Hamiltonian formulation. The new results reported here can be viewed as an extension to consider the significant influence of the cylinder density on the coupled dynamics. We extend the force calculation to axisymmetric flows in § 2. The force is equal to the rate of decrease of the total impulse, and has an intuitively clear form. Combined with an advection equation for point and ring vortices, the coupled dynamics may be followed. This framework is applied to study the coupled dynamics of a cylinder/point vortex (§ 3), a cylinder/dipolar vortex (§ 4), and a sphere/vortex ring (§ 5). The nature of the coupled dynamics is significantly altered by the relative density of the body to the fluid. We show how momentum can be permanently transferred between the body and vortices in a manner altogether different from a drag force. In § 6, we make some general conclusions and attempt to draw a connection with other fluid mechanical problems.

2. Force on a body moving near a singular distribution of vorticity

We calculate the force on a body in the presence of a singular distribution of vorticity where the flow is irrotational except at singular points, lines or surfaces. We focus on point symmetric bodies (cylinders or spheres) which are not rotating and as such we do not consider the torque on such bodies since it is zero in an inviscid fluid. To simplify the analysis we also restrict our attention to a stagnant ambient flow. The analysis may be extended to a steady ambient stream, but the methodology does not readily extend to spatially varying external flows. This point is discussed in § 6.

First, consider a planar body moving with velocity $\boldsymbol{U}$ in an unbounded flow near a collection of N point vortices of circulation Γ_i located at $\boldsymbol{x}_i$, where $i = 1, \ldots, N$. The irrotational flow, $\boldsymbol{u}$, outside the point vortices is related to the pressure field, p, through Euler's equation:

$$\rho \frac{\mathrm{D}\boldsymbol{u}}{\mathrm{D}t} = -\nabla p, \tag{2.1}$$

where ρ is the fluid density. The force on a body located at $\boldsymbol{X}_b$ and moving with velocity $\boldsymbol{U} = \dot{\boldsymbol{X}}_b$ is equal to the normal pressure force integrated over the surface of

the body (S_b):

$$\boldsymbol{F} = \int_{S_b} p\hat{\boldsymbol{n}}\,\mathrm{d}S, \tag{2.2}$$

where $\hat{\boldsymbol{n}}$ is the unit vector normal to the surface of the body and directed into the body.

Because of incompressibility and irrotationality, the velocity can be expressed in terms of a potential which satisfies Laplace's equation. The flow is decomposed as

$$\boldsymbol{u} = \nabla(\phi_b + \phi_v + \phi_i), \tag{2.3}$$

where ϕ_b, ϕ_v and ϕ_i correspond to the velocity potential associated with the bound, free and image vorticity, respectively (using the terminology of Saffman 1992 and Howe 1995). The bound vorticity is generated by the motion of the body. The flow induced by the free vorticity, $\nabla\phi_v$, is calculate using the Biot-Savart Law (Batchelor 1967, p. 507). The kinematic condition applied on the surface of the body is

$$\nabla\phi_b \cdot \hat{\boldsymbol{n}} = \boldsymbol{U} \cdot \hat{\boldsymbol{n}}, \qquad \nabla(\phi_v + \phi_i) \cdot \hat{\boldsymbol{n}} = 0, \tag{2.4}$$

where $\hat{\boldsymbol{n}}$ is a unit normal into the body or out of the control volume encapsulating the body. By applying the momentum integral theorem to (2.1) (e.g. Howe 1995), the difference between the force on the control surface S_∞ and the body is equal to

$$\int_{S_\infty} p\hat{\boldsymbol{n}}\,\mathrm{d}S + \boldsymbol{F} = -\int_{\mathrm{V}_\infty - \mathrm{V}_b} \rho\left(\frac{\partial \boldsymbol{u}}{\partial t} + (\boldsymbol{u}\cdot\nabla)\boldsymbol{u}\right)\mathrm{d}V. \tag{2.5}$$

The body and vortices are enclosed by a large control volume V_∞ which is bounded by the surface S_∞. Integrating (2.1) yields Bernoulli's equation

$$p = -\tfrac{1}{2}\rho u^2 - \rho\frac{\partial \phi}{\partial t} + F(t), \tag{2.6}$$

(Saffman 1992, p. 19). We identify separately the linear impulse associated with the bound, free and image vorticity, defined here by

$$\dot{\boldsymbol{I}}_b = \int_{S_b} \rho\phi_b\hat{\boldsymbol{n}}\,\mathrm{d}S, \qquad \boldsymbol{I}_v = \int_{V_\infty - V_b} \rho\boldsymbol{x}\times\boldsymbol{\omega}\,\mathrm{d}V, \qquad \boldsymbol{I}_i = \int_{S_b} \rho\phi_i\hat{\boldsymbol{n}}\,\mathrm{d}S, \tag{2.7}$$

respectively. (These definitions are equivalent if we explicitly describe the body and image velocity potential in terms of bound/free vorticity.) The impulse associated with the bound vorticity corresponds to the impulse of the body. The density of the fluid is explicitly included here in the definitions of impulse, though in general it is not (see Eames & Hunt 2004 who discuss the effect of ρ changing with time).

The force on the body is therefore determined by the rate of decrease of the total impulse of the flow (see Appendix A):

$$\boldsymbol{F} = -[\dot{\boldsymbol{I}}_b + \dot{\boldsymbol{I}}_v + \dot{\boldsymbol{I}}_i], \tag{2.8}$$

where the impulse of the body, $\boldsymbol{I}_b$, is determined by its velocity and geometry, characterized in terms of the added-mass tensor $\boldsymbol{C}_m$, through

$$\boldsymbol{I}_b = \rho\boldsymbol{C}_m V_b \cdot \boldsymbol{U}. \tag{2.9}$$

Thus,

$$(\rho_b\boldsymbol{I} + \rho\boldsymbol{C}_m)V_b \cdot \dot{\boldsymbol{U}} = -\dot{\boldsymbol{I}}_v - \dot{\boldsymbol{I}}_i, \tag{2.10}$$

where $\boldsymbol{I}$ is the identity matrix. Equation (2.15) is identical to the result of Shashikanth *et al.* (2002), Milne-Thompson (1968) and Sarpkaya & Garrison (1963). Howe's (1995)

general expression for the force on a body, implicitly suggests (2.10). Integrating (2.10) with time gives

$$[(\rho_b \boldsymbol{I} + \rho \boldsymbol{C}_m) V_b \cdot \boldsymbol{U} + \boldsymbol{I}_v + \boldsymbol{I}_i]_0^t = 0. \tag{2.11}$$

The above expression has a clear physical interpretation, with the sum of the momentum of the body and the total impulse of the flow being conserved. It is the simple form of (2.11) which enables us to study analytically the coupled dynamics of isolated bodies and singular distributions of vorticity. The analyses of Shashikanth (2005, 2006) also obtain the result (2.11) which forms the basis of his Hamiltonian formation.

In a planar flow, the ith vortex is advected with a velocity

$$\dot{\boldsymbol{x}}_i = \nabla \phi_b(\boldsymbol{x}_i) + \sum_{k=1, k\neq i}^{N} \frac{(\boldsymbol{x}_i - \boldsymbol{x}_k) \times \Gamma_k \hat{\boldsymbol{z}}}{2\pi |\boldsymbol{x}_i - \boldsymbol{x}_k|^2} + \nabla \phi_i(\boldsymbol{x}_i), \tag{2.12}$$

induced locally at the position of the vortex due to the body, other vortices and image vortices. To illustrate the richness of the coupled dynamics, we consider an isolated cylinder (of radius a) moving in an unbounded flow. A cylinder moving with velocity $\boldsymbol{U}$, characterized by $\boldsymbol{C}_m = \boldsymbol{I}$, generates a flow

$$\phi_b(\boldsymbol{x}) = -\frac{a^2 \boldsymbol{U} \cdot (\boldsymbol{x} - \boldsymbol{x}_b)}{|\boldsymbol{x} - \boldsymbol{x}_b|^2}. \tag{2.13}$$

The image and free vorticity generated by point vortices are, respectively, described by the velocity potentials

$$\phi_i(\boldsymbol{x}) = \sum_{k=1}^{N} \frac{\Gamma_k}{2\pi} \log |\boldsymbol{x} - \boldsymbol{x}_b| - \sum_{k=1}^{N} \frac{\Gamma_k}{2\pi} \log \left| \boldsymbol{x} - \boldsymbol{x}_b - \frac{(\boldsymbol{x}_k - \boldsymbol{x}_b) a^2}{|\boldsymbol{x}_k - \boldsymbol{x}_b|^2} \right|, \tag{2.14}$$

$$\phi_v(\boldsymbol{x}) = \sum_{k=1}^{N} \frac{\Gamma_k}{2\pi} \log |\boldsymbol{x} - \boldsymbol{x}_k|, \tag{2.15}$$

(see Saffman 1992). The above results extend naturally to vortex sheets and other singular distributions of vorticity, that may be viewed as a collection of point or line vortices.

For three-dimensional flows, the rate of change of the impulse associated with the free vorticity is

$$\dot{\boldsymbol{I}}_v = \frac{\mathrm{d}}{\mathrm{d}t} \int_{V_\infty - V_b} \tfrac{1}{2} \rho \boldsymbol{x} \times \boldsymbol{\omega} \, \mathrm{d}V = \int_{V_\infty - V_b} \rho \boldsymbol{u} \times \boldsymbol{\omega} \, \mathrm{d}V, \tag{2.16}$$

(from Saffman 1992, p. 58). Repeating the same steps described above for three-dimensional bodies in the presence of singular distributions of vorticity also yields (2.11). Wells (1996) calculated the force on a sphere fixed near a line vortex and discussed a geometrical interpretation of the force, but did not consider the unsteady flow problem. The second example we shall consider is the three-dimensional interaction between a rigid sphere (of radius a) and a thin cored vortex ring. A rigid sphere moving with velocity $\boldsymbol{U}$, characterized by $\boldsymbol{C}_m = \boldsymbol{I}/2$, generates a flow described by the velocity potential

$$\phi_b(\boldsymbol{x}) = -\frac{a^3 \boldsymbol{U} \cdot (\boldsymbol{x} - \boldsymbol{x}_b)}{2|\boldsymbol{x} - \boldsymbol{x}_b|^3}. \tag{2.17}$$

To simplify the analysis, we will restrict our attention to the axisymmetric interaction between a vortex ring and a sphere. The image vorticity for a vortex ring may be obtained from Lighthill (1956*a*), which, together with the self-induced motion (Appendix B) and (2.11), enables the coupled dynamics to be studied, as described in § 5.

3. Interaction between a cylinder and an isolated point vortex

We now examine the coupled dynamics of a point vortex of circulation Γ and a rigid cylinder, which are initially located at $(R, 0)$ and the origin, respectively. Since we focus on the case with zero total momentum, the cylinder must have an initial vertical velocity, $\dot{Y}_b(0)$, which is determined by the initial position of the point vortex. This case can be easily extended to one in which the initial total momentum is non-zero. The position of the vortex and cylinder are denoted by (x_v, y_v) and (X_b, Y_b), respectively, in Cartesian coordinates. Initially, the vortex and cylinder are located at $(R, 0)$ and $(0, 0)$, respectively. The conservation of momentum results in

$$\dot{X}_b = -\frac{\Gamma}{\pi(\rho_b/\rho+1)a^2}\left(y_v - \frac{(y_v - Y_b)a^2}{r_v'^2}\right), \quad \dot{Y}_b = \frac{\Gamma}{\pi(\rho_b/\rho+1)a^2}\left(x_v - \frac{(x_v - X_b)a^2}{r_v'^2}\right). \tag{3.1}$$

The separation between the centre of the cylinder and the point vortex is $r_v' = [(x_v - X_b)^2 + (y_v - Y_b)^2]^{1/2}$. The velocity of the point vortex, $(\dot{x}_v, \dot{y}_y)$, is determined from (2.12)–(2.15). The coupled dynamics are more readily studied in complex variables, where the position of the cylinder's centre, point vortex and separation are $Z_b = X_b + \mathrm{i}Y_b$, $Z_v = x_v + \mathrm{i}y_v$ and $Z = Z_v - Z_b$, respectively. The momentum and advection equations describing the motion of the body and vortex, (3.1) and (2.12) respectively, reduce to

$$\dot{Z}_b = \frac{\Gamma \mathrm{i}}{\pi a^2(\rho_b/\rho+1)}\left(Z - \frac{Za^2}{|Z|^2} + Z_b\right), \tag{3.2}$$

$$\dot{Z} = -\frac{\Gamma \mathrm{i} a^2}{2\pi}\frac{Z}{|Z|^2(|Z|^2 - a^2)} - \frac{\Gamma \mathrm{i}}{\pi a^2(\rho_b/\rho+1)}\left(Z\left(1 - \frac{a^4}{|Z|^4}\right) + Z_b + \frac{\overline{Z_b}}{\overline{Z}^2}\right), \tag{3.3}$$

where $\overline{*}$ denotes the complex conjugate. The separation between the point vortex and cylinder (Z) is determined by the motion of the cylinder (Z_b), but not the image vortices, which induce a flow perpendicular to the line between the cylinder and vortex (i.e. proportional to $\mathrm{i}Z$). The coupled dynamics are controlled by the ratio of the velocity induced by the cylinder (second term on the right-hand side of (3.3)) to the velocity induced by the image vortices (first term on the right-hand side of (3.3)), expressed by $R^4/(\rho_b/\rho+1)a^4$. For $R^4/(\rho_b/\rho+1)a^4 \ll 1$, the initial velocity of the cylinder is sufficiently small that its dynamics are coupled to the point vortex and periodic solutions result. Whereas for $R^4/(\rho_b/\rho+1)a^4 \gg 1$, the cylinder moves sufficiently fast to escape from the vortex and moves off to infinity.

3.1. *Coupled motion:* $R^4/(\rho_b/\rho+1)a^4 \ll 1$

When $R^4/(\rho_b/\rho+1)a^4 \ll 1$, the separation between the vortex and cylinder is sinusoidal, $Z = R\exp(-\mathrm{i}\omega t)$ (from (3.3)), whose angular frequency is,

$$\omega \sim \frac{\Gamma a^2}{2\pi R^2(R^2 - a^2)}. \tag{3.4}$$

From (3.2), the position of the cylinder is

$$Z_b(t) = \frac{2R^4}{a^3(\rho_p/\rho + 1)} \left(1 - \frac{a^2}{R^2}\right)^2 \left(\exp\left(\frac{\Gamma \mathrm{i} t}{\pi(\rho_b/\rho + 1)}\right) - \exp(-\mathrm{i}\omega t)\right). \tag{3.5}$$

According to (3.5), the cylinder moves along an oscillatory path with a mixture of two frequencies: the first is set by the angular frequency of the vortex around the cylinder, and the second, much longer angular frequency, determined by the dipolar response of the cylinder. The position of the vortex is $Z_v = Z + Z_b$. As $\rho_b/\rho \to \infty$, the displacement of the cylinder tends to zero and the vortex moves around the cylinder, recovering the results of Saffman (1996, p. 42) and Howe (2003, p. 111).

The rate of increase of the square of the separation between the vortex and cylinder is

$$\frac{\mathrm{d}|Z|^2}{\mathrm{d}t} = -\frac{\Gamma \mathrm{i}}{a^2\pi(\rho_p/\rho + 1)}(\overline{Z}Z_b - Z\overline{Z_b}) \left(1 - \frac{a^2}{R^2}\right) \sim \frac{4\Gamma R^6(1 - 3a^2/R^2)}{a^6\pi(\rho_b/\rho + 1)^2} \sin(\omega t). \tag{3.6}$$

The separation between the vortex and cylinder oscillates with time. According to (3.6),

$$|Z|^2 = R^2 + \frac{8R^{10}}{a^8(\rho_b/\rho + 1)^2}(1 - \cos\omega t). \tag{3.7}$$

As $R^4/(\rho_b/\rho + 1)a^4$ increases, the amplitude of oscillation of the cylinder (from (3.5) and (3.7)) increases to such an extent that the cylinder moves off to infinity.

3.2. *Uncoupled motion:* $R^4/(\rho_b/\rho + 1)a^4 \gg 1$

When $R^4/(\rho_b/\rho + 1)a^4 \gg 1$, the initial vertical velocity of the cylinder is sufficiently large that it moves off to infinity, and the permanent displacement of the vortex is negligible.

To first order, the cylinder initially moves parallel to the y-axis with a speed $\dot{Y}_b(0) = \Gamma(R - a^2/R)/\pi(\rho_b/\rho + 1)a^2$ (from (3.2)), and the relative separation between the vortex and cylinder increases according to $Z = \dot{Y}_b(0)t\mathrm{i} - R$. From (3.3), the vortex moves ultimately to

$$\lim_{t\to\infty} Z_v(t) \sim Z_v(0) + \int_0^\infty \frac{\Gamma \mathrm{i} a^2}{2\pi} \frac{R - \mathrm{i}\dot{Y}_b(t)t}{(R^2 + \dot{Y}_b^2 t^2)^2}\,\mathrm{d}t = R + \left(-\frac{1}{2} - \frac{\pi}{4}\mathrm{i}\right) \frac{a^4(\rho_b/\rho + 1)}{2R^3}. \tag{3.8}$$

The ultimate velocity of the cylinder is related to the ultimate position of the vortex through (3.1), so that to second order the velocity of the cylinder tends to

$$\frac{\pi a^2(\rho_b/\rho + 1)}{\Gamma} \lim_{t\to\infty} \dot{Z}_b(t) \sim \left(1 - \frac{a^2}{R^2}\right)\mathrm{i} + \left(-\frac{1}{4}\mathrm{i} + \frac{\pi}{8}\right) \frac{(\rho_b/\rho + 1)a^4}{2R^4(1 - a^2/R^2)}. \tag{3.9}$$

For short time, a vortex with positive circulation rotates around the cylinder in a clockwise direction with the vortex initially displaced downwards and horizontally towards the origin. The displacement of the vortex leads to the cylinder, by momentum conservation, acquiring a horizontal velocity while its vertical velocity is slightly reduced, as indicated by (3.9).

3.3. *Numerical results*

Figure 1 shows the trajectories of an isolated point vortex and cylinder calculated numerically for a fixed initial separation ($R = 3a$). Figure 1 shows the influence of decreasing the density of the cylinder, corresponding to an increase in $R^4/(\rho_b/\rho + 1)a^4$. The vortex moves in a clockwise fashion around the cylinder. The cylinder moves in

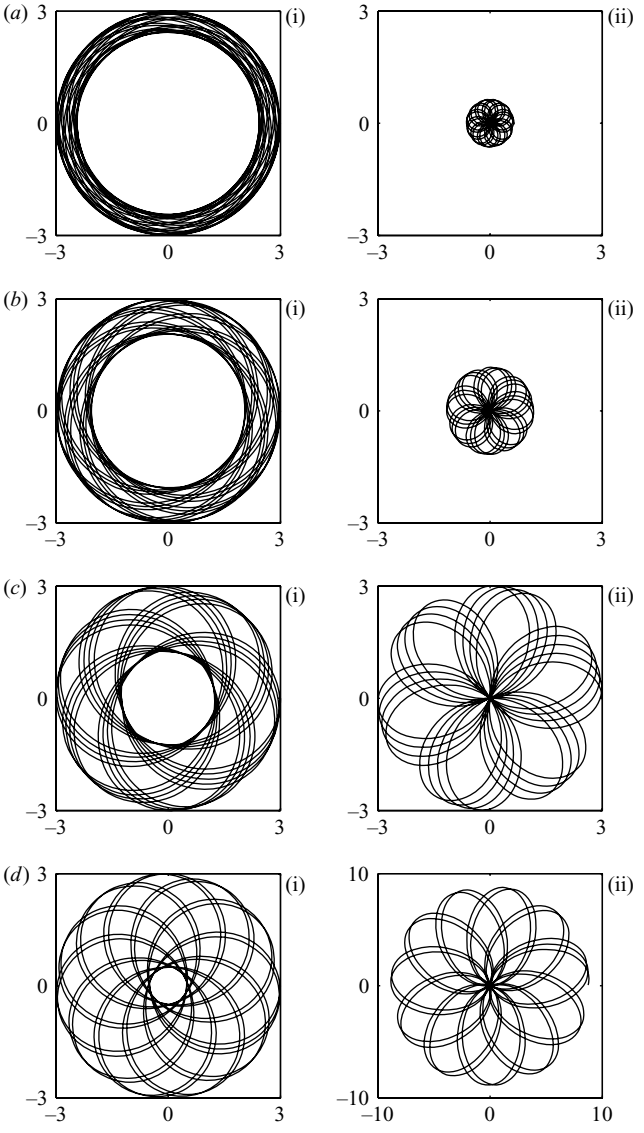

FIGURE 1. The trajectories of the point vortex and cylinder indicated in the left-hand and right-hand columns, respectively. The vortex is initially at $R = 3a$. The figures correspond to (*a*) $\rho_b/\rho = 1000$; (*b*) 500; (*c*) 200; (*d*) 130. Note the contrasting scale in (*d*(*ii*)).

an anticlockwise direction around the origin. With decreasing density of the cylinder, the amplitude of the oscillations increases. This is more clearly illustrated in figure 2 where the corresponding variation of $|Z|^2$ is plotted. For $R^4/(\rho_b/\rho + 1)a^4 \ll 1$, the motion of the cylinder and vortex remain coupled with their separation varying periodically in time.

As the density of the cylinder decreases, a critical value of $R^4/(\rho_b/\rho + 1)a^4$ is reached when the amplitude of the oscillation becomes unbounded. Figure 3 is a regime diagram which discriminates between coupled and uncoupled motion. The critical value of $R^4/(\rho_b/\rho + 1)a^4$ is calculated numerically by first fixing R and then increasing ρ_b/ρ until the separation of the cylinder and vortex exceeds $20R$. For

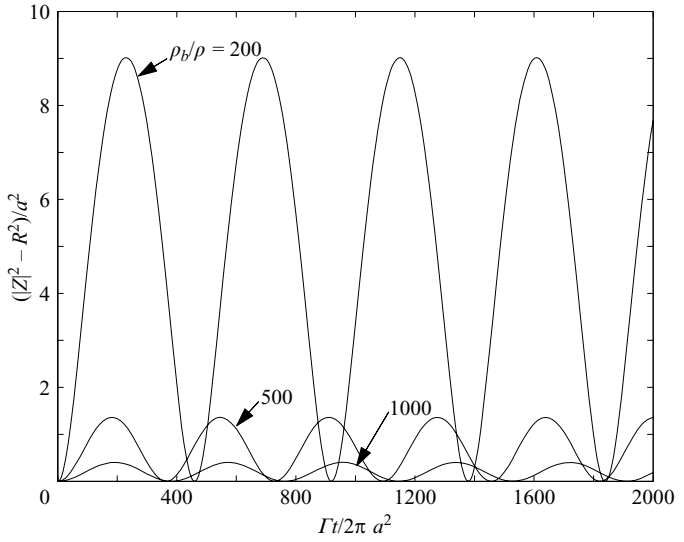

FIGURE 2. The variation of the square of the separation between the cylinder and point vortex, $|Z|^2$, with time, for decreasing values of cylinder density (see figure 1). Note, the result for $\rho_b/\rho = 130$ is not plotted because its amplitude is so much larger that the other examples.

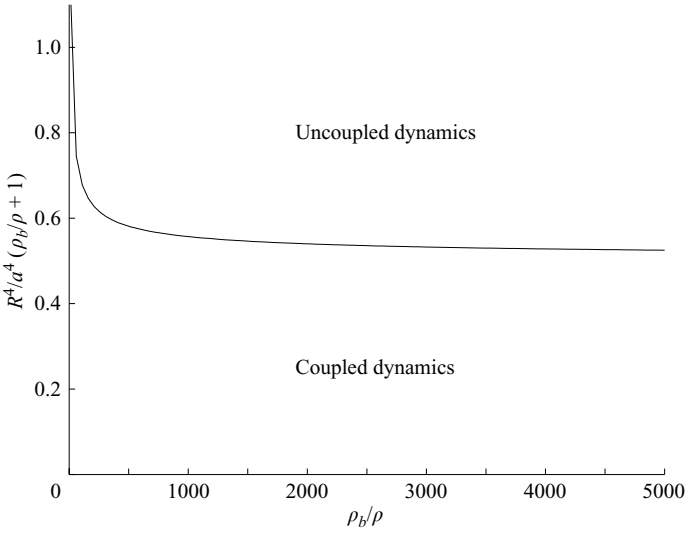

FIGURE 3. Regime diagram describing the dynamics of a cylinder and point vortex.

$\rho_b/\rho \gg 1$, the critical value tends to $R^4/(\rho_b/\rho + 1)a^4 \sim 0.50$. A sensitivity analysis suggests that this critical value hardly changes for larger values than $20R$. The characteristic time scale of the problem is set by a^2/Γ, but the coupled dynamics are independent of the vortex circulation Γ.

When the motion becomes uncoupled, the cylinder acquires a fraction of the vortex impulse and ultimately moves with a constant velocity. Figure 4 shows a hodograph plot of the ultimate dimensionless velocity of cylinders which have moved off to infinity. In the limit of $R^4/(\rho_b/\rho + 1)a^4 \gg 1$, the cylinder moves parallel to the y-axis. The second-order correction to the velocity (3.9) is plotted as a dashed curve and

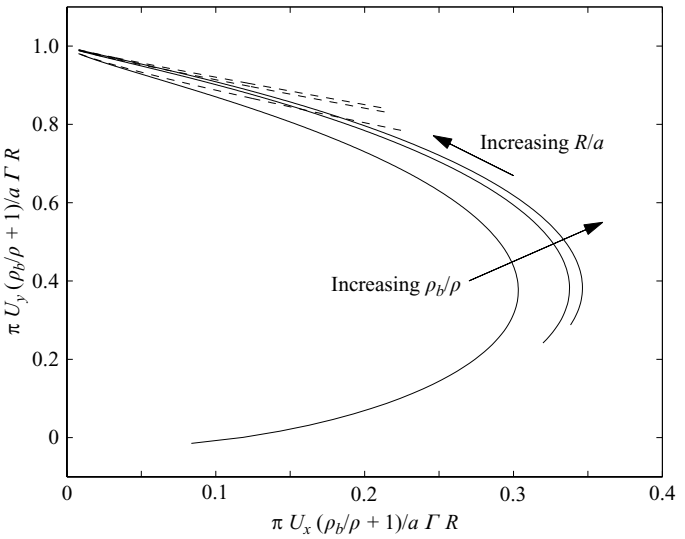

FIGURE 4. Hodograph plot for the velocity of the cylinder which has moved off to infinity. The three curves correspond to $\rho_b/\rho = 100$, 500 and 1000; the initial position of the vortex, R, spans a decade above the critical value indicated in figure 3. As separation between the cylinder and vortex increases, the velocity of the cylinder tends to the dashed curves described by (3.9).

provides a leading-order description when the separation between the vortex and cylinder is initially large.

4. Interaction between a cylinder and a dipolar vortex

We extend the previous calculations to examine the interaction between a cylinder, initially at rest at the origin, and a propagating dipolar vortex starting at infinity. The separation between the positive and negative point vortices, each of absolute strength Γ, is $2d$ and their midpoint is initially a distance h from the centreline.

4.1. *Symmetric interaction* ($h = 0$)

The positive and negative point vortices have positions $(x_v, \pm y_v)$. Far upstream of the cylinder ($x_v \to -\infty$), the separation of the vortices, $2y_v$, tends to $2d$ (figure 5*a*). The cylinder moves along the centreline, with a horizontal velocity related to the impulse of the image and free vorticity through

$$\dot{X}_b = \frac{2\Gamma}{\pi a^2(\rho_b/\rho + 1)}\left[d - y_v\left(1 - \frac{a^2}{r_v'^2}\right)\right], \tag{4.1}$$

where $r_v' = ((x_v - X_b)^2 + y_v^2)^{1/2}$ and $x_v' = x_v - X_b$. By symmetry, we need only consider the motion of the positive vortical element lying in the upper half-plane ($y > 0$), which according to (2.12) moves with a velocity

$$\dot{x}_v = \frac{\Gamma}{2\pi}\left[\frac{1}{2y_v} + \frac{y_v}{r_v'^2 - a^2} - \frac{y_v\left(1 + a^2/r_v'^2\right)}{x_v'^2\left(1 - a^2/r_v'^2\right)^2 + y_v^2\left(1 + a^2/r_v'^2\right)^2}\right] + \frac{\dot{X}_b a^2\left(x_v'^2 - y_v^2\right)}{r_v'^4} \tag{4.2}$$

$$\dot{y}_v = \frac{\Gamma x_v'}{2\pi}\left[-\frac{1}{r_v'^2 - a^2} + \frac{1 - a^2/r_v'^2}{x_v'^2\left(1 - a^2/r_v'^2\right)^2 + y_v^2\left(1 + a^2/r_v'^2\right)^2}\right] + \frac{2\dot{X}_b a^2 x_v' y_v}{r_v'^4}. \tag{4.3}$$

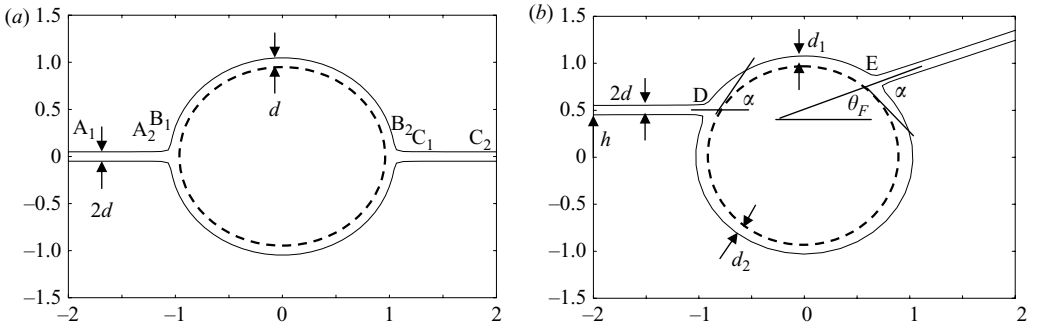

FIGURE 5. Schematic showing the notation employed to study (*a*) symmetric ($h = 0$) and (*b*) asymmetric interaction ($h > 0$) between a cylinder (denoted by a dashed line) and a dipolar vortex whose trajectory is denoted by a thin line. These problems are studied in §§4.1 and 4.2, respectively. In (*a*), points A_2B_1 and B_2C_1 are, respectively, $(r_1, \pi - \theta_1)$ and (r_1, θ_1). In (*b*), the angular deflection of the vortex is θ_F.

In this problem, the cylinder is initially at rest and so has zero initial impulse and momentum. As we shall see, the interaction between the dipolar vortex and cylinder has two possible outcomes: the dipolar vortex moves over and past the cylinder and does not impart impulse to the cylinder, or the cylinder acquires impulse, and moves off to infinity faster than the dipole.

4.1.1. *Asymptotic expressions for displacement in the limits of* $d/a \ll 1$, $\rho_b/\rho \gg 1$

This limit corresponds to a dense cylinder and a small vortex. As the vortex approaches the cylinder, the impulse associated with the image dipolar vortex decreases, so that the cylinder initially moves forward. Within a distance $\sim d$ from the cylinder's centre (corresponding to A_2B_1 in figure 5*a*), the vortical elements separate and pass (along B_1B_2) around the cylinder, increasing the impulse of the dipolar vortex, and the velocity of the cylinder decreases until its direction of motion is reversed. Along B_1B_2, vortices lie a distance $\sim d$ from the cylinder – they unite at B_2C_1 before moving off at a constant speed.

We assume *a priori* that the cylinder is displaced a small distance forward ($|X_b| \ll a$), and confirm this assumption at the end of this calculation. When $|X_b| \ll a$, the trajectory of the vortices are described (Milne-Thompson 1968, p. 369), to leading order, in polar coordinates, by

$$r_v \sin\theta_v \left(1 - \frac{a^2}{r_v^2}\right) = d\left(1 + \frac{a^4}{r_v^4} - \frac{2a^2}{r_v^2}\cos 2\theta_v\right)^{1/2}. \tag{4.4}$$

The dynamics of the cylinder may be calculated by considering the vortex trajectory along the sections A_1A_2, B_1B_2 and C_1C_2 (see figure 5*a*), and matching asymptotic expansions over an intermediate region. The vortex dipole spends a finite time $O(d^2/\Gamma)$ near to A_2B_1 and B_2C_1, so that a regular perturbation analysis may be applied to estimate the displacement of the cylinder – this is in contrast to fluid particles which spend an infinite time near stagnation points and for which a matched asymptotic analysis must be applied (Lighthill 1956*b*).

Along the trajectories A_1A_2 and C_1C_2, the radial velocity of the vortex is

$$\dot{r}_v = \frac{\Gamma \cot\theta_v}{4\pi r_v}\left(1 - \frac{4d^2a^2}{\left(r_v^2 - a^2\right)^2}\right). \tag{4.5}$$

The displacement of the cylinder as the point vortex moves from A_1 to A_2, can be estimated by combining (4.1), (4.4) and (4.5) to yield

$$X_{b,A_1A_2} = \int_{r_1}^{\infty} \frac{\dot{X}_b}{\dot{r}_v}\,\mathrm{d}r_v \sim \frac{8}{a^2(\rho_b/\rho+1)} \int_{r_1}^{\infty} r_v \tan\theta_v \frac{d - r_v \sin\theta_v \left(r_v^2 - a^2\right)/r_v^2}{1 - 4d^2/\left(r_v^2 - a^2\right)^2}\,\mathrm{d}r_v, \quad (4.6)$$

where $(r_1 - a)/a \ll 1$. Expanding the integrand in terms of $r_v (\sim d/\sin\theta_v)$ and integrating, we obtain

$$X_{b,A_1A_2} \sim \frac{8d^2}{a(\rho_b/\rho+1)}. \quad (4.7)$$

As the point vortex moves from A_1 to A_2, the impulse of the image vorticity decreases, so that the cylinder acquires impulse and moves forward.

Along the curved trajectory B_1B_2, the radial positions of the vortical elements are

$$r_v \sim a + d - \frac{d^2}{2a} + \frac{d^3}{2a^2 \sin^2\theta_v}. \quad (4.8)$$

From (4.8) and (4.1), the cylinder's velocity is

$$\dot{X}_b \sim \frac{2\Gamma d}{\pi a^2(\rho_b/\rho+1)} (1 - 2\sin\theta_v). \quad (4.9)$$

As the vortical elements pass around the cylinder, the angular position of the positive vortex decreases (from $\theta_v = \pi$) leading to a decrease in the cylinder's velocity. Over the range $\pi/6 \leqslant \theta_v \leqslant 5\pi/6$, the impulse of the free vorticity increases to such an extent that the velocity of the cylinder is negative. From (4.2) and (4.3), the angular speed of the vortex around the cylinder is

$$\dot{\theta}_v \sim -\frac{\Gamma a}{4\pi r_v^2 (r_v - a)}. \quad (4.10)$$

Combining (4.9) and (4.10), the displacement of the cylinder due to the vortex moving along B_1B_2 is

$$X_{b,B_1B_2} = \int_{\pi-\theta_1}^{\theta_1} \frac{\dot{X}_b}{\dot{\theta}_v}\,\mathrm{d}\theta_v \sim \frac{8d^2(4-\pi)}{a(\rho_b/\rho+1)}, \quad (4.11)$$

where $\theta_1 \ll 1$. The total displacement of the cylinder is obtained by combining contributions from A_1A_2, B_1B_2 and C_1C_2, to yield

$$\lim_{t\to\infty} X_b(t) = 2X_{b,A_1A_2} + X_{b,B_1B_2} \sim \frac{8(\pi-2)d^2}{a(\rho_b/\rho+1)}, \quad (4.12)$$

as $d/a \to 0$. Equation (4.12) ensures that $|X_b| \ll a$ and the initial assumption is then justified.

4.1.2. *Asymptotic expressions for displacement in the limits of* $d/a > 1$, $\rho_b/\rho \gg 1$

When the vortex is no longer small, the displacement of the cylinder must also be considered. The main steps in the analysis of the cylinder displacement are described. To first order, the velocity of the cylinder is described (from § 4.1.1) by

$$\dot{X}_b \sim \frac{2\Gamma d}{\pi a^2(\rho_p/\rho+1)} \left[\frac{a^2}{r_v^2}\cos 2\theta_v - \frac{a^4}{2r_v^4}\sin^2 2\theta_v + \cdots\right]. \quad (4.13)$$

To leading order, the velocity and displacement of the cylinder are

$$\dot{X}_{b1} = \frac{2\Gamma d}{\pi a^2(\rho_p/\rho + 1)} \frac{a^2}{r^2} \cos 2\theta_v, \qquad X_{b1} = \frac{4d}{\rho_p/\rho + 1} \sin 2\theta_v. \tag{4.14}$$

By integrating (4.13), the permanent displacement, to first order, is

$$\lim_{t\to\infty} X_b \sim \frac{7\pi a^2}{d(\rho_p/\rho + 1)}. \tag{4.15}$$

The velocity of the cylinder is determined, to second order, by relaxing the constraint that the cylinder is fixed, to give (from (4.1)),

$$\dot{X}_b \sim \frac{2\Gamma}{\pi a^2(\rho_b/\rho + 1)} \left(d - y_v \left(1 - \frac{a^2}{r_v^2} \right) + \frac{2x_v y_v X_{b1} a^2}{r_v^4} \right). \tag{4.16}$$

The vertical velocity of the vortical element, expanded about the origin, is

$$\dot{y}_v(x_v', y_v) \sim \dot{y}_v(x_v, y_v) + X_{b1} \frac{\partial \dot{y}_v}{\partial x_v}, \tag{4.17}$$

which yields

$$\begin{aligned} \dot{y}_v \sim & -\frac{2\Gamma \sin^2\theta_v \cos\theta_v}{\pi r_v^3} + \frac{2\sin\theta_v \cos\theta_v a^2 \dot{X}_{b1}}{r_v^2} + \frac{6\Gamma X_{b1} \sin^2\theta_v \cos^2\theta_v}{\pi r_v^4} \\ & + \frac{2\Gamma X_{b1} \sin\theta (2\sin\theta_v \cos^2\theta_v - \sin^3\theta_v)}{\pi r_v^4}. \end{aligned} \tag{4.18}$$

Likewise, to second order, the angular velocity of the vortex around the cylinder is

$$\dot{\theta}_v \sim -\frac{\Gamma}{4\pi r_v^2} \left(1 + \frac{4a^2 \sin^2\theta_v}{r_v^2} \right) + \frac{\dot{X}_{b1} \sin\theta}{r_v^3} + \frac{\Gamma X_{b1} \sin^2\theta_v \cos\theta_v}{\pi r_v^5}. \tag{4.19}$$

By combining (4.18) and (4.19), the vertical position of the positive point vortex is

$$y_v = \int_\pi^0 \frac{\dot{y}_v}{\dot{\theta}_v} \, \mathrm{d}\theta \sim d + \frac{2a^2 \sin^4\theta_v}{d} + \frac{a^2}{d(\rho_p/\rho + 1)} [4\sin^4\theta_v + 48\sin^6\theta_v - 48\sin^8\theta_v]. \tag{4.20}$$

Substituting (4.20) into (4.16) and integrating using (4.19), the displacement of the cylinder is now

$$\lim_{t\to\infty} X_b(t) \sim \frac{7\pi a^2}{(\rho_p/\rho + 1)d} + \frac{24\pi d}{(\rho_p/\rho + 1)^2}. \tag{4.21}$$

Rescaling (4.21) results in

$$\tilde{X}_b = \lim_{t\to\infty} X_d(t) \frac{(\rho_b/\rho + 1)^{3/2}}{a\pi(168)^{1/2}}, \qquad \tilde{d} = \frac{(24/7)^{1/2} d}{a(\rho_b/\rho + 1)^{1/2}},$$

or

$$\tilde{X}_b \sim \frac{1}{\tilde{d}} + \tilde{d}. \tag{4.22}$$

Thus for $\rho_b/\rho \gg 1$, the displacement of the cylinder is not monotonically increasing with d, but rather displays a local maxima and minima, with the displacement ultimately increasing in proportion to d. The analysis is valid providing the displacement is much smaller than a, a constraint which requires $d/a \ll (\rho_b/\rho + 1)^2$.

When this is not satisfied, the displacement still grows in proportion to d (for $d/a \gg 1$), but with an offset not captured by the analysis described.

4.1.3. *Light cylinder,* $\rho_b/\rho < 1$

As shown in § 4.1.2, the cylinder accelerates forward as the dipolar vortex approaches. If the inertia of the cylinder is small enough, the cylinder acquires sufficient impulse from the dipolar vortex that it moves with the same velocity as the vortex. The flow induced by the cylinder squeezes the vortical elements together, further reducing the impulse of the vortex and increasing the velocity of the cylinder. Finally, the cylinder moves faster than the vortex. This type of encounter is completely different from that for dense cylinders.

For $d/a \gg 1$, the relative velocity between the vortex and cylinder (from (4.1)) is approximately

$$\dot{x}_v - \dot{X}_b \sim \frac{\Gamma}{4\pi y_v} - \frac{2\Gamma}{\pi a^2(\rho_b/\rho + 1)} \left[d - y_v \left(1 - \frac{a^2}{r_v'^2} \right) \right]. \tag{4.23}$$

The point at which the relative speed of the vortex to the cylinder is zero, is determined from (4.20) and (4.23), to be

$$\frac{\rho_b}{\rho} + 1 \sim \left(16 + \frac{160}{\rho_b/\rho + 1} \right) \sin^4 \theta_s + \frac{256}{\rho_b/\rho + 1} \sin^6 \theta_s - \frac{384}{\rho_b/\rho + 1} \sin^8 \theta_s. \tag{4.24}$$

Equation (4.24) indicates that the angular position of the turning-point is independent of the initial size of the vortex. Comparison of (4.24) with numerical solutions confirms that θ_s is accurately predicted for $\rho_b/\rho < 0.1$, but the difference increases to 20 % for $\rho_b/\rho \sim 1$.

4.2. *Asymmetric interaction* ($h > 0$)

For asymmetric interactions between the dipolar vortex and cylinder, both the trajectories of the positive and negative vortical elements must be followed. These equations are not listed here but can be obtained from (2.12)–(2.15).

To illustrate the asymmetric interaction physically, we consider a small dipolar vortex 'striking' a dense cylinder, so that $h \leqslant a$, $\rho_b/\rho \gg 1$ and $d/a \ll 1$. The interaction is relatively local in this case, so that the cylinder can be represented as an inclined wall at point D (figure 5*b*). Denoting the separation of the positive and negative vortices from the cylinder by d_1 and d_2 (see figure 5*b*), we find from impulse and energy conservation during the finite-time interaction with the cylinder (e.g. Batchelor 1967, p. 531; Eames & Dalziel 2000), that

$$d_1 - d_2 = 2d\cos\alpha, \qquad d_1 d_2 = d^2, \tag{4.25}$$

where $\alpha = \cos^{-1}(h/a)$. Since $d_1 > d_2$, the positive vortex moves slower around the cylinder than the negative vortex. The vortices meet at the point E (figure 5*b*) determined by the relative angular velocity of the two vortices around the cylinder, before moving off at an angle α to the local tangent of the cylinder. The dipolar vortex is ultimately deflected by an angle

$$\theta_F = 2\alpha - \frac{2\pi}{\left(\cos\alpha + (\cos^2\alpha + 1)^{1/2}\right)^2 + 1}, \tag{4.26}$$

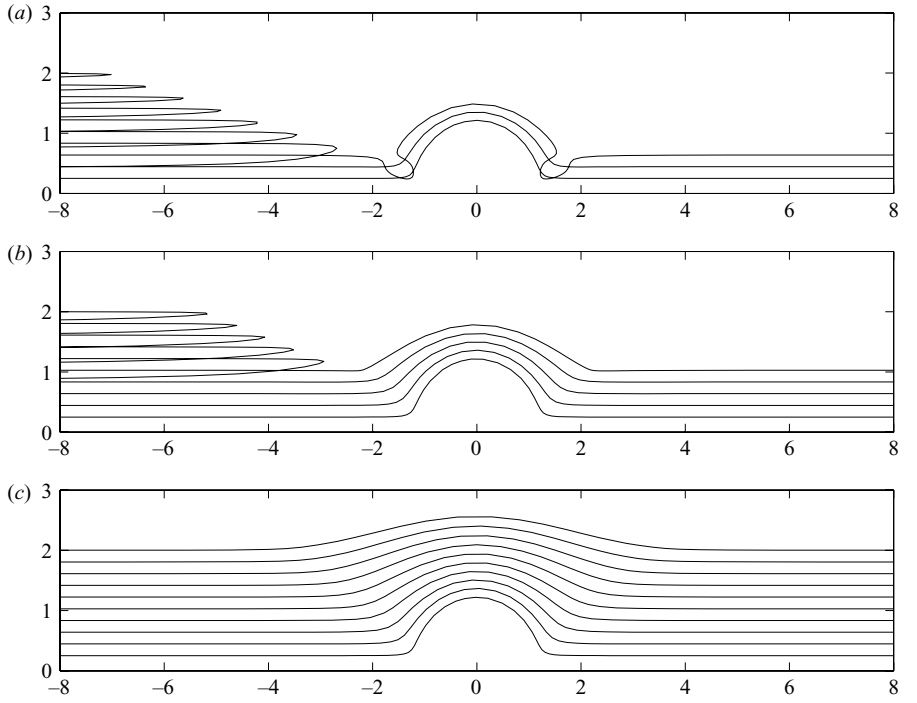

FIGURE 6. Upper half-plane showing the trajectories of dipolar vortices (in the frame of the cylinder) released far upstream of the cylinder, with d/a for (*a*) $\rho_b/\rho = 0$; (*b*) 0.5, and (*c*) 1. For $\rho_b/\rho = 1$, the vortices pass around the cylinder, while for $\rho_b/\rho < 1$, the vortices far from the cylinder reverse with the cylinder moving off to infinity.

to the horizontal, independent of d for $d/a \ll 1$. The ultimate velocity of the cylinder is determined, from (2.10), by the direction of propagation of the vortex through

$$\lim_{t\to\infty} \boldsymbol{U} = \frac{2\Gamma d}{\pi a^2(\rho_b/\rho + 1)} (1 - \cos\theta_F, -\sin\theta_F)\,. \tag{4.27}$$

For $h/a > 1$ and $d/a \ll 1$, the dipolar vortex does not 'strike' the cylinder and the angular displacement of an incident vortex is negligible.

4.3. *Numerical results*

Figure 6 shows the trajectories of the positive vortex for different cylinder densities and separation distances, d. The trajectories are plotted in the frame moving with the cylinder. The velocity of the cylinder increases as the dipolar vortex approaches it, because the impulse of the image vortex decreases. In figure 6(*a*), some trajectories reverse relative to the moving cylinder, illustrating that for large d the cylinder speeds up relative to the vortex, and the cylinder acquires impulse. For small d, the impulse exchange during interaction is too small to enable the cylinder to overtake the dipolar vortex. When the vortex moves around and over the cylinder, the cylinder's impulse reduces to zero and is displaced a finite distance forward. The threshold value of d/a for which the cylinder overtakes the vortex, increases for denser cylinders (see figure 6*b*, *c*), whereas for $\rho_b/\rho \geqslant 1$, all vortices move past the cylinder. A regime diagram showing the transition between these two different interactions is shown in figure 7. The angular position of the vortices relative to the cylinder, and the impulse exchange, represented by the reduction in the vortex separation, is shown in figure 8.

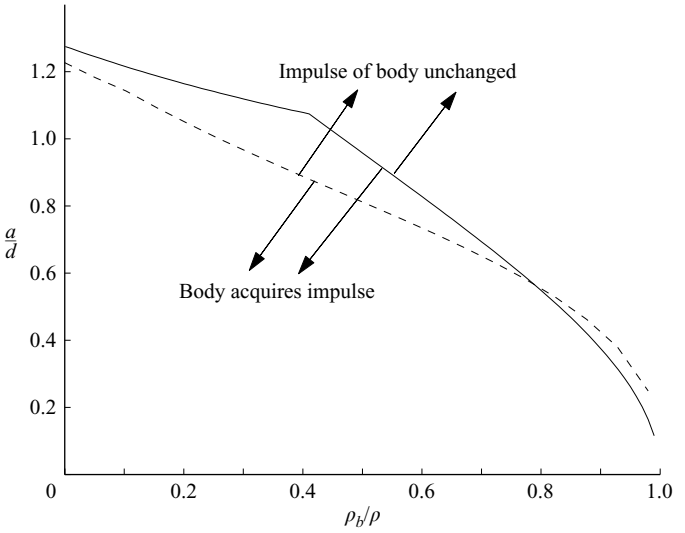

FIGURE 7. Regime diagram for a symmetric dipole and cylinder interaction. The dashed/full curve denotes the separation between two regimes of changed and unchanged vortex impulse for a cylinder/sphere. The regime diagram for a symmetric interaction between a sphere and vortex ring is calculated for a vortex core to sphere radius $r_0/a = 0.1$ (see § 5).

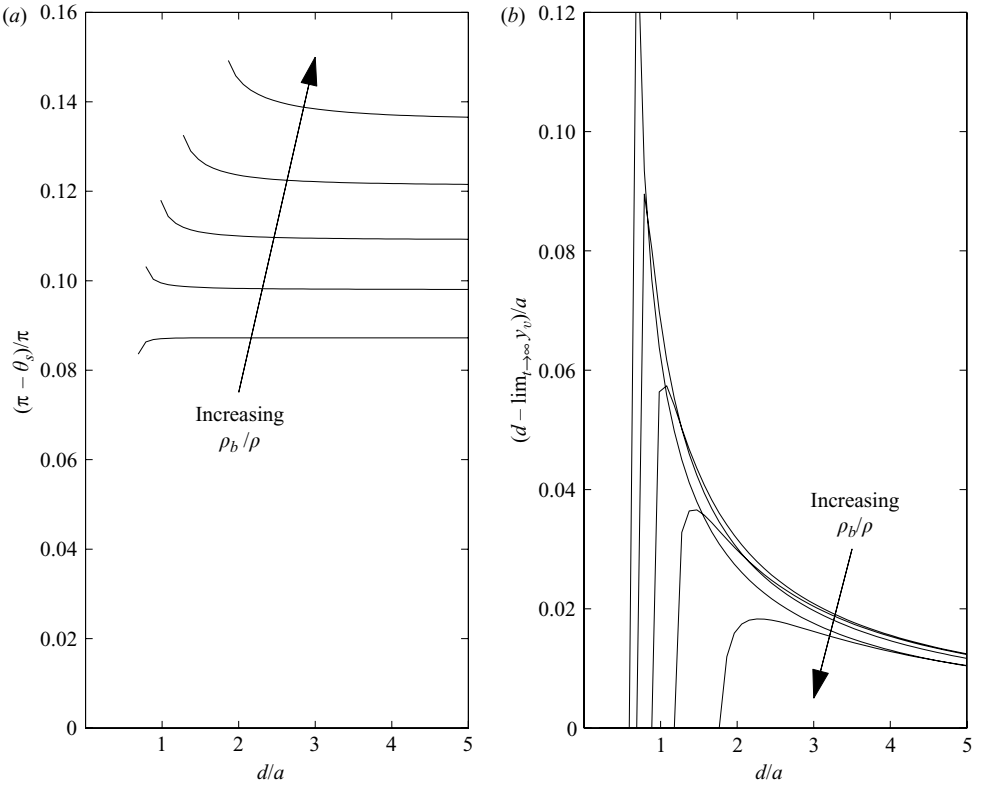

FIGURE 8. The angular position of the point at which the relative velocity of the vortex to the cylinder reverses, as a function of d/a, is shown in (a) for $\rho_b/\rho = 0$, 0.2, 0.4, 0.6 and 0.8. The final impulse of the cylinder is proportional to the reduction in the separation of the vortical elements ($d - \lim_{t\to\infty} y_v$) whose variation with the initial separation of the vortices, $2d$, and cylinder density is shown in (b).

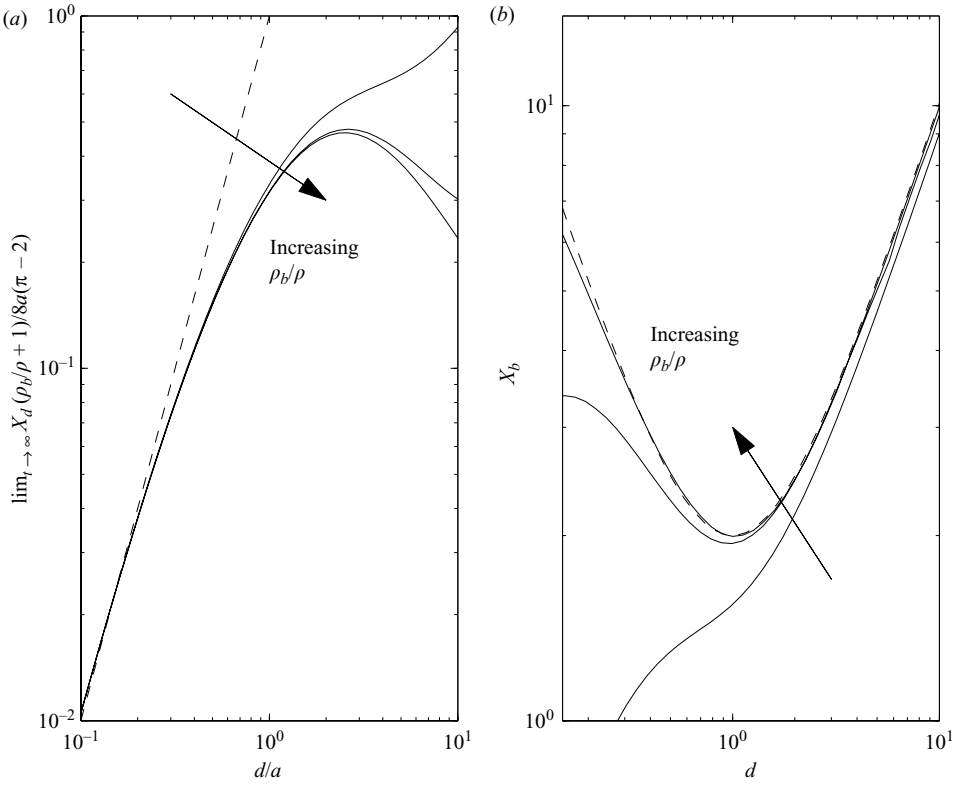

FIGURE 9. Displacement of a dense cylinder, $\lim_{t\to\infty} X_b(t)$ for (*a*) small d/a and (*b*) large d/a, owing to a symmetric interaction with a dipolar vortex, for $\rho_b/\rho = 10^2, 10^3$ and 10^4. The displacement is normalized to enable (4.12) and (4.22), plotted as dashed lines in (*a*) and (*b*), respectively, to be tested. In (*b*), only a few of the displacement curves are plotted.

Figure 9 shows the total displacement of a dense cylinder caused by a symmetric interaction with a dipolar vortex ($h = 0$), as a function of the initial size of the vortex. For $d/a \ll 1$, the permanent displacement increases with d and figure 9(*a*) shows good agreement with the prediction (4.12). The displacement does not increase monotonically with d, but for large values of ρ_b/ρ has a point of inflection. The rescaled displacement shown in figure 9(*b*) is in agreement with (4.22) for dense cylinders.

The angular deflection of the dipolar vortex θ_F following an encounter with a dense cylinder is shown in figure 10. The angular displacement depends on the incident angle to the cylinder. The relative travel times of the positive and negative vortical elements around the cylinder correspond, respectively, to the first and second terms in (4.26). For small h/a, the first contribution in (4.26) dominates. For larger $h/a < 1$, the relatively faster speed of the positive vortical element determines the position of the encounter between the two elements and thereby also θ_F. The agreement with the predictions (4.26) and numerical results appears good for $d/a \ll 1$ and $h/a < 1$. For large h/a, the angular displacement of the dipolar vortex is small.

5. Interaction between a sphere and vortex ring

The crucial difference between vortex–body interactions in two- and three-dimensions is the rate of decay of velocity perturbations with distance. To illustrate

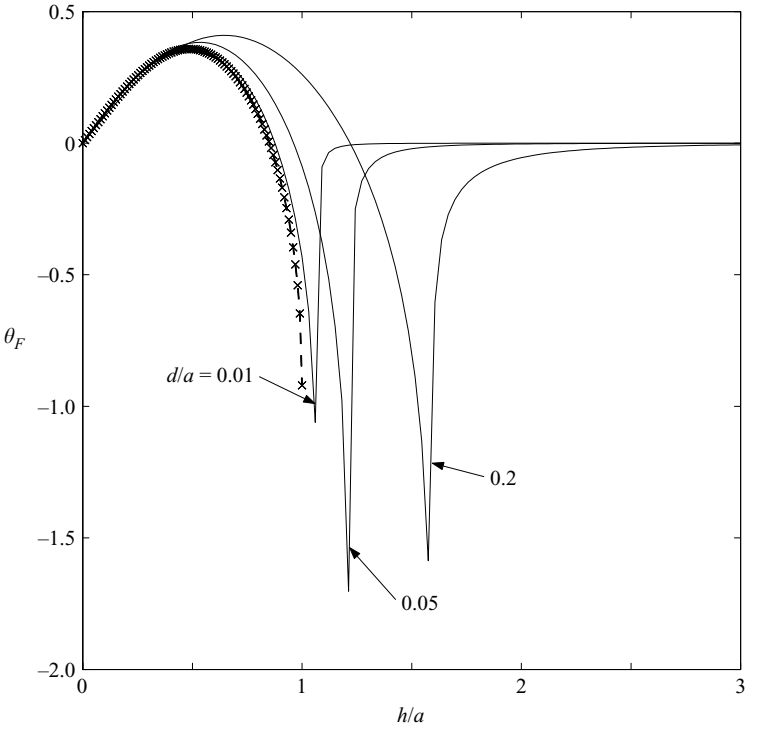

FIGURE 10. The variation of the angular deflection, θ_F, of a dipolar vortex with h/a (see figure 5*b*), for $d/a = 0.01, 0.05$ and 0.2. The density of the cylinder is fixed at $\rho_b/\rho = 100$. $\times$, approximation (4.26) to the angular deflection.

that, broadly, the results for two- and three-dimensions are consistent, we consider the symmetric interaction between a rigid sphere (of radius a), initially at rest, and a vortex-ring. The vortex-ring starts from infinity, has circulation Γ, initial radius d and core radius r_0 and position x_v, y_v. Because of the presence of the sphere, an image vortex ring of circulation $\Gamma' = -\Gamma r_v'/a$, and radius $a^2 y_v/r_v'^2$ is created, where $r_v' = ((X_b - x_v)^2 + y_v^2)^{1/2}$.

The conservation of momentum (2.15), gives

$$\frac{4\pi a^3}{3}\left(\frac{\rho_b}{\rho} + C_m\right)\dot{X}_b = \pi\Gamma\left(d^2 - y_v^2\left(1 - \frac{a^3}{r_v'^3}\right)\right), \tag{5.1}$$

where $C_m = 1/2$. The vortex ring is advected with a velocity $(\dot{x}_v, \dot{y}_v)$ where

$$\dot{x}_v = \frac{a^3\dot{X}_b(2x_v'^2 - y_v^2)}{2r_v'^5} + u_{vx} + U_v, \tag{5.2}$$

$$\dot{y}_v = \frac{3a^3\dot{X}_b x_v' y_v}{2r_v'^5} + u_{vy}. \tag{5.3}$$

The flow induced by the image vortex ring, (u_{vx}, u_{vy}), is described in Appendix B. The self-induced velocity of the vortex ring,

$$U_v = \frac{\Gamma}{4\pi y_v}\left[\ln\left(\frac{8d}{r_0}\left[\frac{y_v}{d}\right]^{3/2}\right) - \frac{1}{4}\right], \tag{5.4}$$

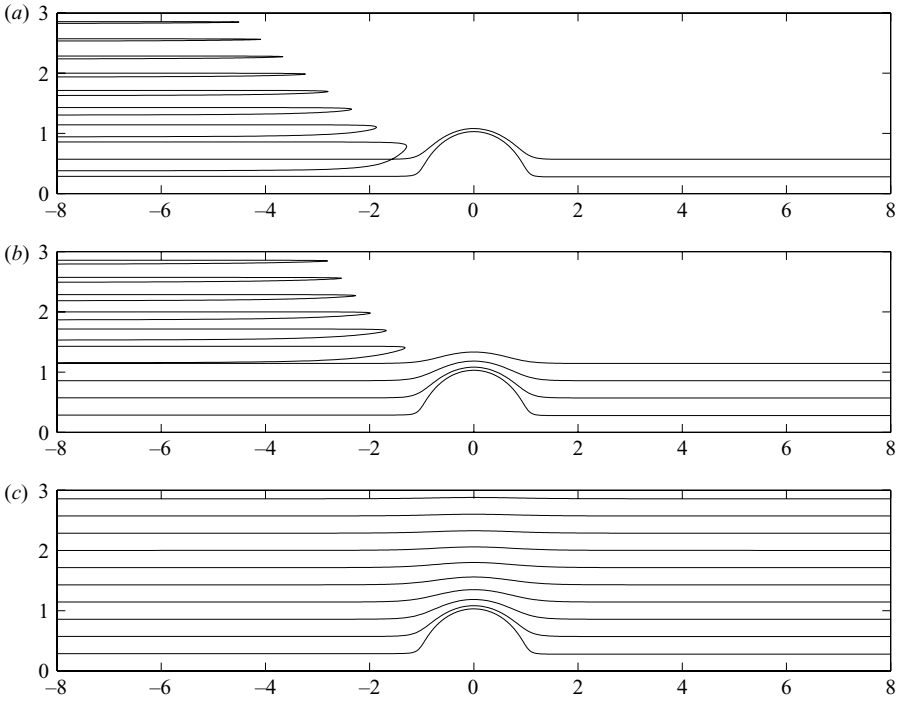

FIGURE 11. Trajectories of a vortex ring which encounters a sphere, in the frame of the sphere, for (*a*) $\rho_b/\rho = 0$; (*b*) 0.5 and (*c*) 1.

is based on an assumption that the vortex core is much smaller than its radius (i.e. $r_0/d \ll 1$) and that it remains circular with time. An identical set of equations have been applied to explore the interaction between vortex rings and spheres (Howe 2003). The new aspect of the present calculation is the inclusion of the coupled momentum equation (5.1) and the sphere's density. Figure 11 shows the trajectories of a vortex ring, in the frame moving with the sphere, for $\rho_b/\rho = 0$, 0.5 and 1. As for the two-dimensional cylinder interactions above, a light sphere may acquire impulse from the vortex ring before moving off faster than the vortex. Figure 7 shows a regime diagram which discriminates between when impulse is transferred from the vortex ring to the sphere and when the impulse of the vortex ring is preserved. This faster decay ensures that the interaction occurs much closer to the sphere, as shown by comparing figure 11(*a*) and figure 6(*a*). The fractional reduction in the radius of the vortex ring is shown in figure 12(*b*). Note that for $\rho_b/\rho < 1.5$, the sphere can acquire impulse from the vortex; but for $\rho_b/\rho \gg 1$, the vortex moves over the sphere, which is permanently displaced a finite distance forward.

When the vortex ring is large ($d/a \gg 1$), and the sphere dense ($\rho_b/\rho \gg 1$) the velocity of the vortex perpendicular to the centreline is

$$\dot{y}_v = -\frac{3y^3 x \Gamma a^3}{4(x^2 + d^2)^4}. \tag{5.5}$$

To leading order, the translation velocity of the vortex ring is unchanged for $d/a \gg 1$, and the perturbation to the radius of the vortex ring is

$$y_v \sim d + \frac{d^2 a^3 \Gamma}{8U_v(x^2 + d^2)^3}. \tag{5.6}$$

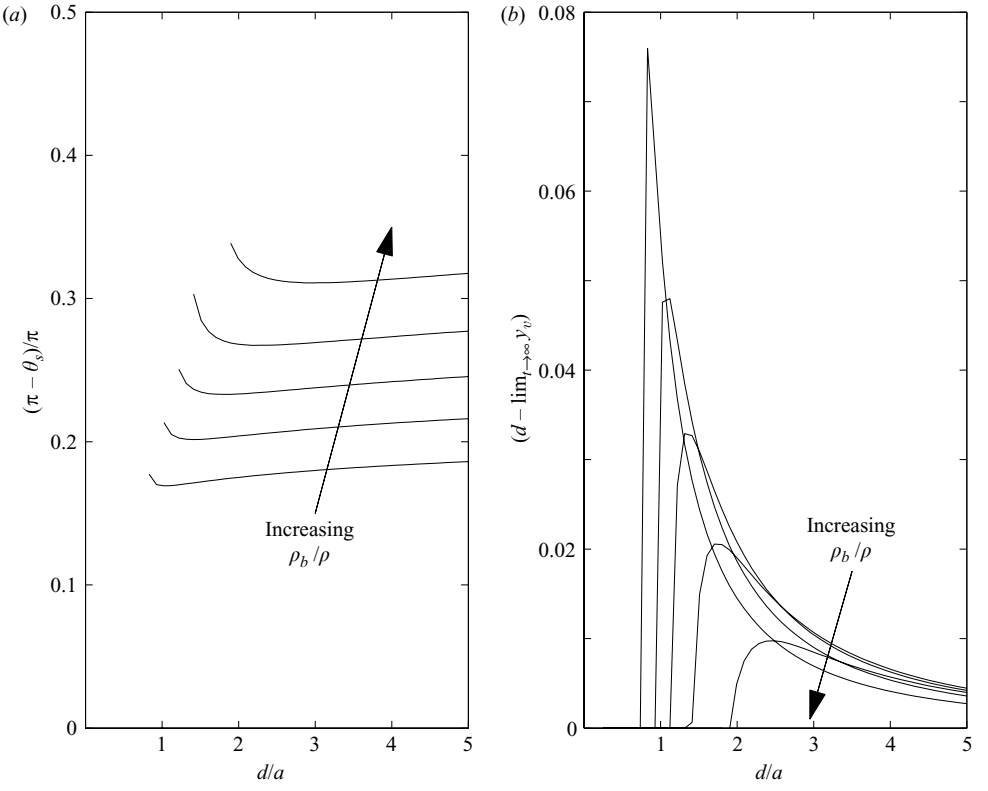

FIGURE 12. (*a*) Angular position of the stationary point where the vortex trajectory reverses. (*b*) The permanent decrease in the vortex radius as a consequence of interacting with a sphere, as a function of its initial size, is shown. The density of the sphere is $\rho_b/\rho = 0, 0.2, 0.4, 0.6$ and 0.8.

Substituting (5.6) into (5.1), we obtain a leading-order estimate for the displacement of the sphere:

$$\lim_{t\to\infty} X_b(t) \sim \frac{d}{\rho_b/\rho + C_m}\left(\frac{3}{2(U_v d/\Gamma)} - \frac{9\pi}{128(U_v d/\Gamma)^2}\right). \tag{5.7}$$

Numerical calculations show that the displacement of a dense sphere increases monotonically with d, in contrast to the displacement of a dense cylinder. The local interaction means that (5.7) provides a leading-order description of displacement (figure 13).

6. Concluding remarks

The motivation for this study was to understand (*a*) how rigid bodies move near flow features whose length scale is comparable to, or smaller than, the size of the body, and (*b*) how they permanently modify the flow. This has been illustrated with examples of a cylinder or sphere moving inviscidly near singular distributions of vorticity. The motion of the body and vortices is controlled by the conservation of the momentum of the body and total impulse of the flow.

The density of the body critically alters the coupled dynamics: a light cylinder (or sphere) symmetrically interacting with a dipolar vortex (or vortex ring) extracts a

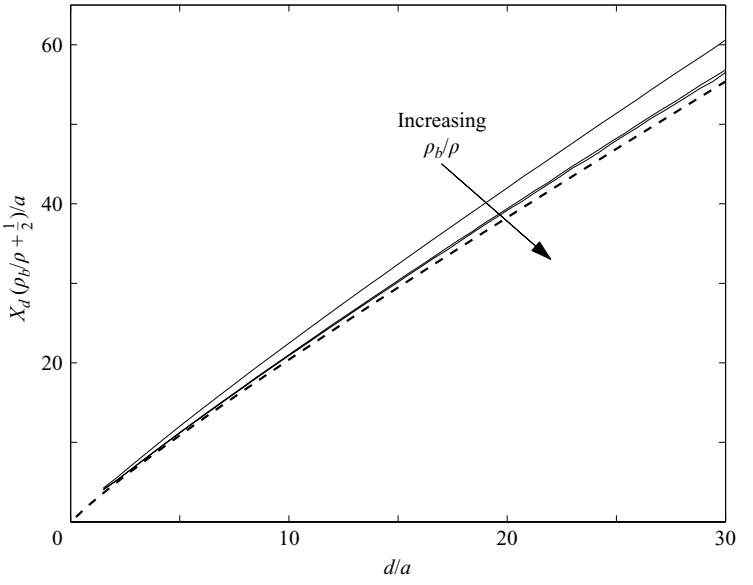

FIGURE 13. Displacement of a dense sphere owing to a symmetric interaction with a vortex ring of radius d and a core radius $r_0/a = 0.1$. The dashed curve is the asymptotic expression (5.7) for displacement, and the full lines correspond to the numerical solutions for $\rho_b/\rho = 100$, 200 and 1000.

fraction of the vortex impulse, and moves off at a constant velocity, faster than the vortex. In contrast, a dense cylinder (or sphere) does not extract impulse from the dipole vortex (or vortex ring), but is instead displaced a finite distance forward. The asymmetric interaction between an initially stationary cylinder and vortex dipole is reminiscent of two colliding particles, both being governed by momentum conservation: a dipolar vortex striking a cylinder asymmetrically is deflected, with the cylinder acquiring a horizontal and vertical velocity which depends on the angular deflection of the vortex. The inviscid interaction represents a general mechanism by which bodies may acquire, or even lose momentum, by permanently communicating it to the vortical field. This is an altogether different mechanism than momentum exchange through a drag force, which tends to reduce the slip velocity between bodies and the flow.

This inviscid analysis was based on an assumption that the vorticity distribution is singular in order that the body/vortex coupling could be studied analytically. Although the analysis can be applied when there is an external uniform flow, by a non-inertial change of frame, this cannot be so readily applied to inhomogeneous ambient flows. To extend this analysis to arbitrarily shaped bodies requires both the force and torque on the body to be calculated. (The torque on two-dimensional bodies in the presence of point vortices is known (Shashikanth *et al.* 2002), but the corresponding result for three-dimensional bodies is not.)

Impulse is conserved in unbounded viscously dominated flows, but not when sources of vorticity from rigid surfaces are present. Therefore, (2.10) does not apply to viscous flows. The influence of vorticity generation by rigid surfaces can be significant, as illustrated by Orlandi (1993) for a laminar dipolar vortex striking a rigid fixed cylinder. Secondary vorticity created on the cylinder's surface pairs up with opposite-signed vorticity from the incident vortex. The elements of the incident vortex ultimately

separate. This is in contrast to the inviscid calculations for a dense cylinder which show that the vortical elements move around the cylinder and unite before moving off to infinity. For problems where the shed vorticity can be estimated or modelled (e.g. Sarpkaya 1963; Obasaju, Bearman & Graham 1988; McLain & Rock 1996), the analysis presented can provide practical estimates of the forces on rigid bodies. For some problems, where the generation of shed vorticity from surfaces is weak, such as from the surface of clean spherical bubbles, we would expect the analysis to provide a leading-order description of the coupled motion of bubbles and vortices. Despite these limitations, for inertially dominated flows, the drag and lift forces on steadily translating bodies can be calculated from (2.8) by considering the impulse flux in the far field, providing a simplified method, for instance, of estimating the shear lift force calculated by Auton (1987).

The analysis presented provides new insight into how bodies and a vortical field are coupled. Such processes are neglected from current two-phase flow theories, except through momentum exchange terms generally based on the drag on the dispersed phase. In this example, the momentum exchange depends on the time history of the flow, rather than on an instantaneous relative slip between the discrete phases. Although such processes are negligible for dilute particle-laden flows, they become increasingly important for liquid and bubbly flows, where inertial forces are important. A significant future challenge remains how to correctly incorporate this information into Lagrangian models of turbulent two-phase flows.

Finally, the analysis suggests that the free dynamics of rigid bodies and vortices are sensitive to the density of the bodies relative to the ambient flow when $\rho_b/\rho < 1$. Govardhan & Williamson (2002) report a critical change in the behaviour of freely moving cylinders at $\rho_b/\rho = 0.54$. For $\rho_b/\rho < 0.54$, the amplitude and frequency of oscillation increases dramatically suggesting that the cylinders extract a proportion of the impulse of the shed vortices and communicate this to the lift force.

Appendix A

From (2.5),

$$\int_{S_\infty} p\hat{\boldsymbol{n}}\,\mathrm{d}S + \boldsymbol{F} = -\rho\frac{\mathrm{d}}{\mathrm{d}t}\int_{V_\infty - V_b} \boldsymbol{u}\,\mathrm{d}V - \rho\int_{S_\infty} (\boldsymbol{u}\cdot\hat{\boldsymbol{n}})\boldsymbol{u}\,\mathrm{d}S. \tag{A 1}$$

Decomposing $\boldsymbol{u}$ into bound, free and image contributions, the first terms on the right-hand side of (A 1) are

$$-\frac{\mathrm{d}}{\mathrm{d}t}\int_{S_b}(\phi_b+\phi_i)\hat{\boldsymbol{n}}\,\mathrm{d}S - \frac{\mathrm{d}}{\mathrm{d}t}\int_{S_\infty}(\phi_b+\phi_i)\hat{\boldsymbol{n}}\,\mathrm{d}S$$
$$-\frac{\mathrm{d}}{\mathrm{d}t}\left\{\int_{V_\infty - V_b}\boldsymbol{x}\times\boldsymbol{\omega}\,\mathrm{d}V + \int_{S_\infty}\boldsymbol{x}\times(\hat{\boldsymbol{n}}\times\nabla\phi_v)\,\mathrm{d}S\right\},$$

(using identity (16) Saffman 1992, p. 65).

$$\boldsymbol{F} = -\frac{\mathrm{d}}{\mathrm{d}t}\int_{S_b}\rho(\phi_b+\phi_i)\hat{\boldsymbol{n}}\,\mathrm{d}S - \frac{\mathrm{d}}{\mathrm{d}t}\int_{V_\infty - V_b}\rho\boldsymbol{x}\times\boldsymbol{\omega}\,\mathrm{d}V + \rho\boldsymbol{E}, \tag{A 2}$$

where

$$\boldsymbol{E} = -\int_{S_\infty}\left(\tfrac{1}{2}u^2\hat{\boldsymbol{n}} - (\boldsymbol{u}\cdot\hat{\boldsymbol{n}})\boldsymbol{u}\right)\mathrm{d}S + \frac{\mathrm{d}}{\mathrm{d}t}\int_{S_\infty}\{(\phi_v - \boldsymbol{x}\cdot\nabla\phi_v)\hat{\boldsymbol{n}} + (\boldsymbol{x}\cdot\hat{\boldsymbol{n}})\nabla\phi_v\}\,\mathrm{d}S.$$

The terms can be evaluated on a large circular control volume of radius R_s. For a sufficiently large control surface the first term is zero. When the free vorticity has a non-zero circulation, in the far field $\phi_v \to \sum_i^N \Gamma_i/2\pi \tan^{-1}(y/x)$. Evaluating the second integral term as $R_s \to \infty$, we find it is a constant and finally obtain

$$\boldsymbol{F} = -[\dot{\boldsymbol{I}}_b + \dot{\boldsymbol{I}}_v + \dot{\boldsymbol{I}}_i].$$

In extending the results to three-dimensions, for a vortex ring and body, the only major difference is that the far-field flow is dipolar and there is a factor of 1/2 introduced for the impulse associated with the free vorticity.

Appendix B

The equation describing the flow induced by the image vortex ring is described. The image of a vortex ring located at (x_v, y_v) and a sphere at $(X_b, 0)$ is a vortex ring of circulation $\Gamma' = -\Gamma r'_v/a$ and radius $\hat{y} = y_v a^2/r'^2_v$. The streamfunction describing the flow around the image vortex is

$$\Psi = \frac{\Gamma'(y_v\hat{y})^{1/2}}{2\pi}\left(\left(\frac{2}{k} - k\right)K(k) - \frac{2}{k}E(k)\right), \tag{B 1}$$

where

$$k^2 = \frac{4y_v\hat{y}}{\hat{x}^2 + (y_v + \hat{y})^2}, \qquad \hat{x} = (x_v - X_b)\left(1 - \frac{a^2}{r'^2_v}\right),$$

and $K(k)$, $E(k)$ are the complete Elliptic functions of the first and second kind (see Saffman 1992, p. 193). The velocity components are related to the streamfunction through

$$u_{vx} = -\frac{1}{y}\frac{\partial\Psi}{\partial y}, \quad u_{vy} = -\frac{1}{y}\frac{\partial\Psi}{\partial x}. \tag{B 2}$$

REFERENCES

Auton, T. R. 1987 The lift force on a spherical body in a rotational flow. *J. Fluid Mech.* **183**, 199–218.

Batchelor, G. K. 1967 *An Introduction to Fluid Mechanics*. Cambridge University Press.

Borisov, A. V. & Mamaev, I. S. 2003 An integrability of the problem on the motion of cylinder and vortex in the ideal fluid. *Reg. Chaot. Dyn.* **8**, 163–166.

Dhanak, M. R. 1981 Interaction between a vortex filament and an approaching rigid sphere. *J. Fluid Mech.* **110**, 129–147.

Eames, I. & Dalziel, S. B. 2000 Dust resuspension by the flow around an impacting sphere. *J. Fluid Mech.* **403**, 305–328.

Eames, I. & Hunt, J. C. R. 2004 Forces on bodies moving unsteadily in rapidly compressed flows. *J. Fluid Mech.* **505**, 349–364.

Flór, J. B. & Eames, I. 2002 Dynamics of monopolar vortices on a topographic beta-plane. *J. Fluid Mech.* **456**, 353–376.

Govardhan, R. & Williamson, C. H. K. 2002 Resonance forever: existence of a critical mass and an infinite regime of resonance in vortex-induced vibration. *J. Fluid Mech.* **473**, 147–166.

Hill, R. J., Koch, D. L. & Ladd, A. J. C. 2001 Moderate-Reynolds-number flows in ordered and random arrays of spheres. *J. Fluid Mech.* **448**, 243–278.

Howe, M. S. 1995 On the force and moment on a body in an incompressible fluid, with application to rigid bodies and bubbles at high and low Reynolds numbers. *Q. J. Mech. Appl. Maths* **48**, 401–426.

Howe, M. S. 2003 *Theory of Vortex Sound*. Cambridge University Press.

Howe, M. S., Lauchle, G. C. & Wang, J. 2001 Aerodynamic lift and drag fluctuations of a sphere. *J. Fluid Mech.* **436**, 41–57.

Hunt, J. C. R. 1987 Vorticity and vortex dynamics in complex turbulent flows. *Trans. Can. Soc. Mech. Engrs* **11**, 21–35.

Hunt, J. C. R. & Durbin, P. A. 1999 Perturbed vortical layers and shear sheltering. *Fluid Dyn. Res.* **24**, 375–404.

Juckes, M. N. & McIntyre, M. E. 1987 A high-resolution one-layer model of breaking planetary waves in the stratosphere. *Nature* **305**, 593–600.

Kim, I., Elghobashi, S. & Sirignano, W. A. 1997 Unsteady flow interaction between a pair of advected vortex tubes and a rigid sphere. *Intl J. Multiphase Flow* **23**, 1–23.

Lamb, H. 1932 *Hydrodynamics*. Dover.

Lighthill, M. J. 1956*a* The image system of a vortex element in a rigid sphere. *Proc. Cam. Phil. Soc.* **52**, 317–321.

Lighthill, M. J. 1956*b* Drift. *J. Fluid Mech.* **1**, 31–53. (Corrigenda 1957 *J. Fluid Mech.* **2**, 311–312.)

Lighthill, M. J. 1958 *Introduction to Fourier Analysis and Generalized Functions*. Cambridge University Press.

Linden, P. F. 1973 The interaction of a vortex ring with a sharp density interface: a model for turbulent entrainment. *J. Fluid Mech.* **60**, 467–480.

McLain, T. W. & Rock, S. M. 1996 Experiments in the hydrodynamic modeling of an underwater manipulator. In *Symp. Autonomous Underwater Vehicle Technology, IEEE*, pp. 463–469.

Magnaudet, J. & Eames, I. 2000 The motion of high-Reynolds-number bubbles in inhomogeneous flows. *Annu. Rev. Fluid Mech.* **32**, 659–708.

Masoudi, M. & Sirignano, W. 2002 Collision of a vortex with a vaporising droplet. *Intl J. Multiphase Flow* **26**, 1925–1949.

Milne-Thompson, L. M. 1968 *Theoretical Hydrodynamics*. 4th edn. Macmillan.

Mougin, G. & Magnaudet, J. 2002 Path instability of a rising bubble. *Phys. Rev. Lett.* **88**, 1, 014502.

Obasaju, E. D., Bearman, P. W. & Graham, J. M. R. 1988 A study of forces, circulation and vortex patterns around a circular cylinder in oscillating flow. *J. Fluid Mech.* **196**, 467–494.

Orlandi, P. 1993 Vortex dipoles impinging circular cylinders. *Phys. Fluids.* **5**, 2196–2206.

Pedrizzetti, G. 1992 Close interaction between a vortex filament and a rigid sphere. *J. Fluid Mech.* **245**, 701–722.

Ramodanov, S. M. 2001 Motion of a circular cylinder and a vortex in an ideal fluid. *Reg. & Chaot. Dyn.* **6**, 33–38.

Ramodanov, S. M. 2002 Motion of a circular cylinder and N point vortices in a perfect fluid. *Reg. Chaot. Dyn.* **7**, 291–298.

Rossby, C. G. 1948 On displacements and intensity changes of atmospheric vortices. *J. Mar. Res.* **7**, 175–187.

Saffman, P. G. 1992 *Vortex Dynamics*. Cambridge University Press.

Sarpkaya, T. 1963 Lift, drag and added-mass coefficients for a circular cylinder immersed in a time-dependent flow. *J. Appl. Mech.* **30**, 13–18.

Sarpkaya, T. 1968 An analytical study of separated flow about circular cylinders. *Trans. ASME* D: *J. Basic Engng* **90**, 511–520.

Sarpkaya, T. & Garrison, C. J. 1963 Vortex formation and resistance in unsteady flow. *J. Appl. Mech.* **30**, 16–24.

Shashikanth, B. N. 2005 Poisson brackets for the dynamically interacting system of a 2D rigid cylinder and N point vortices: the case of arbitrary smooth cylinder shapes. *Reg. Chaot. Dyn.* **10**, 1–14.

Shashikanth, B. N. 2006 Symmetric pairs of point vortices interacting with a neutrally buoyant two-dimensional circular cylinder. *Phys. Fluids* **18**, 127103.

Shashikanth, B. N., Marsden, J., Burdick, J. & Kelly, S. 2002 The Hamilitonian structure of a 2-D rigid cylinder interacting dynamically with N point vortices. *Phys. Fluids* **14**, 1214–1228.

Smedman, A.-S., Hogstrom, U. & Hunt, J. C. R. 2003 Effects of shear sheltering in a stable atmospheric boundary layer with strong shear. *Q. J. R. Met. Soc.* **130**(A-596), 31–50.

Squires, K. S. & Simonin, O. 2002 Application of DNS and LES to dispersed turbulent two-phase turbulent flow. *Proc. Tenth Workshop on Two-Phase Flow Predictions, Halle, Germany*.

Wells, J. C. 1996 A geometrical interpretation of force on a translating body in rotational flow. *Phys. Fluids* **8**, 442–450.